The bimodal fluid evolution of the Nimbus Zn-Ag deposit: an Archean VHMS with epithermal characteristics

Stefano Caruso, Marco L Fiorentini, Crystal LaFlamme
Centre for Exploration and Targeting, University of Western Australia, 35 Stirling Highway, Crawley WA 6009, Australia

Steven P Hollis
iCRAG (Irish Centre for Research in Applied Geosciences), School of Earth Sciences, University College Dublin, Belfield, Dublin 4, Ireland

Laure A J Martin
ARC Centre of Excellence for Core to Crust Fluid Systems (CCFS) and Centre Microscopy Characterisation and Analysis, The University of Western Australia, 35 Stirling Highway, Crawley, WA 6009, Australia

Stephen J Barnes
CSIRO Mineral Resources Flagship, Kensington, WA 6151, Australia

Dany Savard
LabMaTer, Universite du Quebec a Chicoutimi, 555 Boulevard Universite, Chicoutimi, QC G7H 2B1, Canada

Paul Gillespie
MacPhersons Resources, Kalgoorlie, WA 6430, Australia

Abstract. The Nimbus Zn-Ag VHMS deposit represents an exceptional mineralised occurrence in the Yilgarn Craton. While other VHMS systems in the craton are restricted to paleo-rift zones, Nimbus is associated to a plume-related stratigraphy (Hollis et al., 2017). Furthermore, the epithermal characteristics resulting from low temperature and shallow water conditions allowed the development of an unusual mineralisation dominated by Ag-rich sulfosalts.
In this study we take advantage of state-of-the-art in-situ techniques to investigate the fluid evolution of this peculiar VHMS system. From the trace element compositions and S-isotope signatures we suggest that Nimbus experienced a bimodal fluid evolution consisting of (i) an initial intense interaction between deep-magmatic fluids and seawater that developed barren pyritic lenses, and (ii) a subsequent closure of the hydrothermal system during which the Ag-rich ore formed sourcing sulfur almost entirely from a deep-magmatic source.

1 Geological setting

In the Archean Yilgarn Craton, volcanic-hosted massive sulfide (VHMS) mineralisation is predominately restricted to zones of thin juvenile crust as recently identified by regional (Nd, Pb and Hf) isotope studies (Huston et al., 2014; Mole et al. 2014). Interpreted as Archaean paleo-rift zones, one such zone trends N-S through the Eastern Goldfields Superterrane and is associated with the high grade ca. 2690 Ma Teutonic Bore, Jaguar and Bentley VHMS deposits (Hollis et al., 2015). Until recently, the plume-related lower portions of the stratigraphy were considered unprospective since only minor VMS-like occurrences (e.g. historic Anaconda mine) and barren pyritic lenses were recognised.

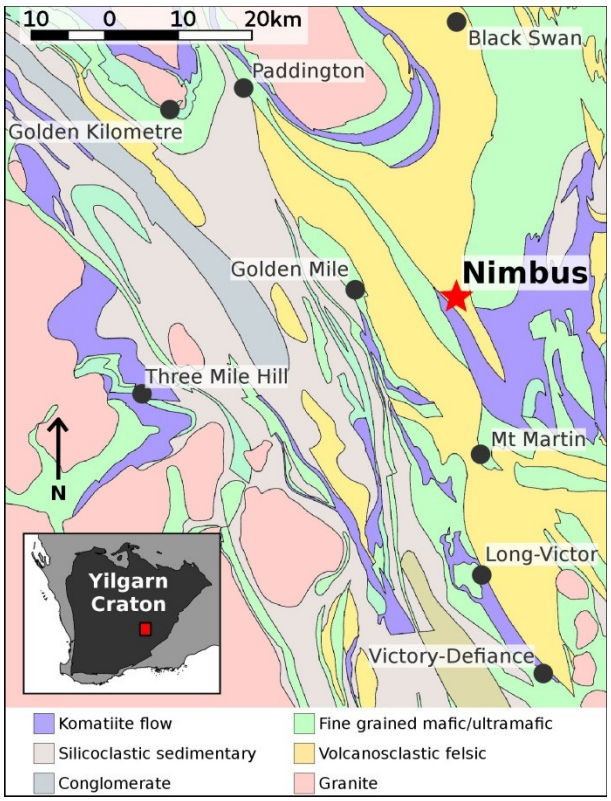

Figure 1. Modified section of the 1:500.000 geological map of Western Australia provided by the Geological Survey of Western Australia.

The Nimbus Ag-Zn-(Au) VHMS deposit, located approximately 10 km east of Kalgoorlie (Figure 1), represents the first notable exception to this paradigm. It is hosted in a NW-trending and steeply-dipping bimodal-felsic package of volcanic rocks with a FI-affinity (felsic volcanic rocks, ocean-plateau like low-Th basalts, Piercey, 2011) which have been identified as coeval with the 2704 Ma plume magmatism responsible for world-class Ni-komatiite mineralisation (Hollis et al., 2017).

The mineralisation, assessed at 12.1 Mt at 52 g/t Ag, 0.9% Zn and 0.2 g/t Au, consists of a series of stacked plunging sulfide-bearing lenses. The ore mineralogy is characterised by sphalerite associated with abundant Ag-Sb-Pb-As sulfosalts, arsenopyrite and rare chalcopyrite. The intense and pervasive hydrothermal alteration affecting the deposit is dominated by quartz-sericite-carbonate assemblage that shift to chlorite predominantly in the basalt. These features, largely preserved after a low greenshist metamorphic overprinting, have been interpreted by Hollis et al. (2017) as the result of a shallow water and low temperature VHMS system with the Nimbus deposit consequently showing hybrid epithermal characteristics.

2 Methodology

Thirty-five samples representing the different sulfide occurrences were systematically examined by reflected light microscopy.

The mineral chemistry of sulfides and sulfosalts were defined by Wavelength Dispersion Spectrometry (WDS) analyses using a JEOL 8530F microprobe at the Centre for Microscopy, Characterisation and Analysis (CMCA), University of Western Australia. S, As, Sb, Se, V, Fe, Ti, Au, Te, Cu, Pb, Ni, Zn, Co, Ag, Cd, Bi and Hg were quantified following the analytical conditions illustrated in Hassan and Roberts (2017).

Trace elements in pyrite and sphalerite were acquired by Laser Ablation Inductively Coupled Mass Spectrometry (LA-ICP-MS) performed at UQAC-LabMaTer, Université du Québec à Chicoutimi, Canada. ^{34}S, ^{51}V, ^{53}Cr, ^{57}Fe, ^{59}Co, ^{60}Ni, ^{65}Cu, ^{66}Zn, ^{69}Ga, ^{74}Ge, ^{75}As, ^{85}Rb, ^{88}Sr, ^{90}Zr, ^{95}Mo, ^{107}Ag, ^{111}Cd, ^{118}Sn, ^{121}Sb, ^{125}Te, ^{137}Ba ^{157}Gd, ^{178}Hf, ^{181}Ta, ^{182}W, ^{195}Pt, ^{202}Hg, ^{205}Tl, ^{208}Pb, ^{209}Bi, ^{232}Th and ^{238}U were collected following a procedure similar to the one described in Duran et al. (2015).

Quadruple sulfur isotope (^{32}S, ^{33}S, ^{34}S, and ^{36}S) analyses were collected with the CAMECA IMS1280 large-geometry ion probe at the CMCA. In-situ S-isotope measurements were acquired on pyrite, chalcopyrite, arsenopyrite and pyrrhotite with the use of matrix-matched reference materials following the analytical procedure described in LaFlamme et al. (2016).

3 Ore mineralogy and mineral chemistry

At Nimbus the hydrothermal mineralisation occurs in lenses with distinct compositions.

Several lenses are composed of massive pyrite seemingly replacing quartz-feldspar phyric dacite (Figure 2). Such textures display a characteristic “colloform” morphology even though they formed by replacement and not through open-space precipitation. Barren “colloform” pyrite present three subsequent stages of crystallisation identifiable as: (a) early pyrite forming inclusion-rich aggregates on which grown (b) radial clean pyrite and a (c) late stage pyrite related to a series of crack-seal events that fragmented the previous texture.

Ore-bearing lenses consist of a sphalerite, pyrite assemblage associated with polymetallic sulfides, galena and arsenopyrite. Sulfides and sulfosalts occur with a variety of textures that range from massive to infilling brecciated dacite, stockwork, vein and stringer.

The microprobe study of sphalerite and pyrite established the absence of chemical zonation at the micron scale. It also provided reliable quantifications of the major and minor elements that validated the in-situ trace element data acquired by LA-ICP-MS.

Furthermore, EPMA analyses allowed the accurate determination of the chemical composition of several sulfosalts such as Ag-rich boulangerite ($Pb_{4.21}Sb_{4.09}Ag_{0.97}S_{11.03}$), bournonite (stoichiometric - $PbCuSbS_3$), pyrostilpnite ($Ag_{2.94}Pb_{0.06}Sb_{1.19}S_3$), Ag,Zn-rich tetrahedrite ($Ag_{2.36}Zn_{0.58}Cu_{7.20}$,$Fe_{1.76}Sb_{3.98}S_{13}$) and previously unrecognized Zn,Bi-rich meneghinite ($Pb_{13.46}Cu_{0.45}Zn_{0.20}Sb_{7.55}Bi_{0.11}S_{23.96}$).

Sporadic pyrite-bearing siltstone which displays peperitic relationships to both mafic and felsic units occurs within the mine sequence, indicating all were broadly coeval. Sedimentary-hosted pyrites are evenly spread in the silicate groundmass and present a distinct cubic shape.

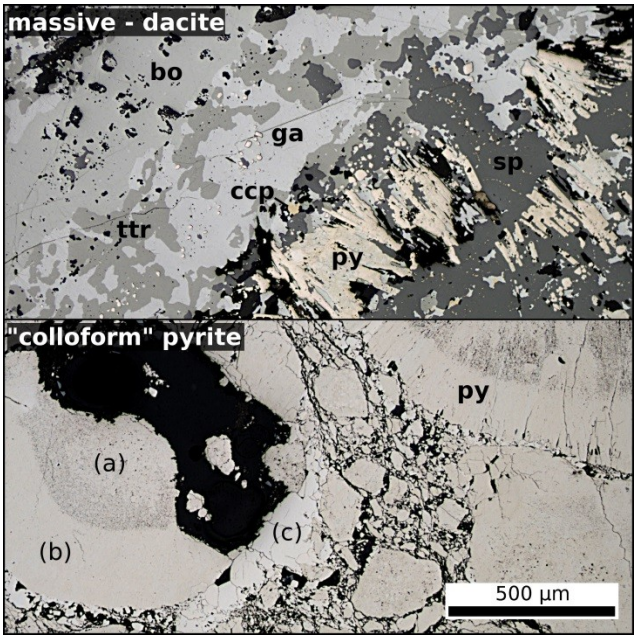

Figure 2. Optical reflected light pictures of representative sulfide textures. Abbreviations are bo – boulangerite, ttr – tetrahedrite, ccp – chalcopyrite, sp – sphalerite, py – pyrite.

4 Multiple S-isotopes systematic

The results from multiple S-isotopes analyses reveal different signatures for each of the main sulfide occurrences (Figure 3).

The "colloform" pyrite is characterised by a negative $\Delta^{33}S$ ranging from -1.71 to -0.15‰ (mean -0.80‰) and by a wide variation in $\partial^{34}S$ from -4.61 to 5.01‰.

Sulfide associated with the Zn-Ag mineralisation display a consistent "near-ZERO" $\Delta^{33}S$ signature averaging at 0.11‰ with few outliers attaining positive values up to 0.42‰ (Figure 4). Ore related sulfides spread on the $\partial^{34}S$ axis between -4.79 and 5.72‰ with positive values prevailing the negatives. Interestingly, negative $\partial^{34}S$ signatures are carried by arsenopyrite and only occasionally by pyrite. Regardless of the ore-textures, the analysed samples equally cover the $\partial^{34}S$ spread with the exception of stringer sulfides that show a distinct positive $\partial^{34}S$ signature of about 4‰.

Analyses on pyrite in siltstone cluster with both $\Delta^{33}S$ and $\partial^{34}S$ positive values at about 3.12 and 5.31‰ respectively.

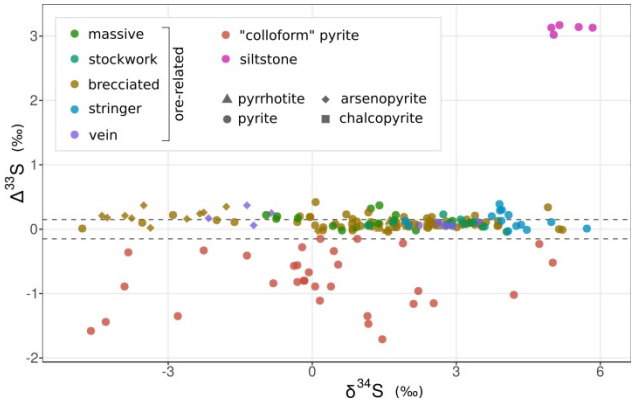

Figure 3. Multiple sulfur isotope results represented as $\Delta^{33}S$ vs $\delta^{34}S$. Dashed lines at ±0.15‰ of $\Delta^{33}S$ delimit the boundaries of non-atmospheric signatures as discussed by Johnstone (2011).

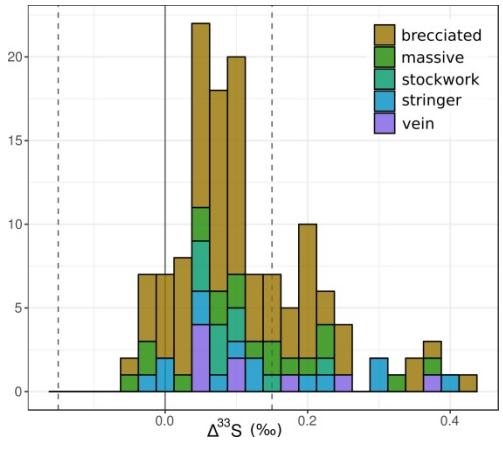

Figure 4. Distribution of $\Delta^{33}S$ values in ore-related samples.

5 In situ LA-ICP-MS analyses

5.1 Trace elements in pyrite

Sediment-hosted pyrite displays an average trace element concentration of 1154ppm with a standard deviation of 330ppm. In particular average concentrations of Sb, As, Pb, and Ni reach 40, 677, 90 and 308ppm respectively.

In comparison with siltstone-hosted pyrite, massive "colloform" pyrite presents a slightly lower trace element content of 1109ppm and a larger standard deviation of 520ppm. Higher contents were measured in the early pyrite aggregates (see "a" in Figure 2) and in the fibrous and concentrically pyrite (see "b" in Figure 2). On average concentrations of Sb, As, Pb, and Ni attain 256, 550, 100 and 175ppm respectively.

Ore-related pyrite presents an irregular distribution for most of the trace elements due to the presence of numerous outliers greater by two to three orders of magnitude. Such anomalous concentrations, likely to be due to sulfosalt inclusions, lead the average trace element concentration to 4421ppm with a standard deviation of 12680ppm. Stringer pyrite are an exception to this paradigm showing a consistent high Ni content that attains concentration up to thousand parts per million (Figure 5).

5.2 Trace elements in sphalerite

The sphalerite trace element content is characterised by a consistent Ag content of about 25ppm and levels of Cd, Hg and Pb attaining 1005, 1665, 1185ppm respectively. In particular, the level of Cd and Hg are largely variable among samples but consistent within the samples (Figure 5). Moreover, the Cd-Hg ratio varies among samples regardless of the sulfide textures.

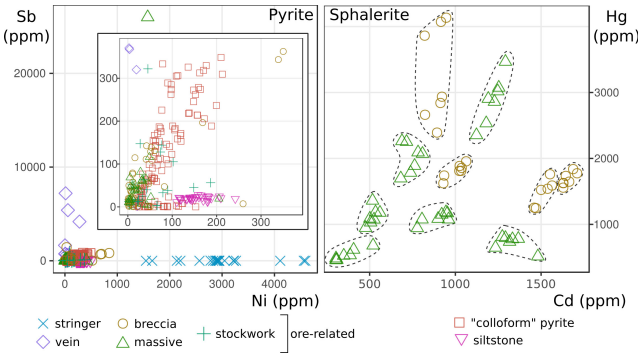

Figure 5. Selected trace element composition of pyrite and sphalerite determined by LA-ICP-MS. For Cd vs Hg in sphalerite the circles contains analyses from the same sample.

6 Discussion

The combination of in-situ techniques for characterising the sulfide trace element contents and S-isotope signatures allows insight pertaining to the fluid evolution of VHMS deposits or more generally hydrothermal systems (e.g. Sharman et al., 2015).

At Nimbus, barren pyrite lenses are characterised by a

consistent negative $\Delta^{33}S$ signature that testify a major input of sulfur derived from Archean seawater sulfate (Farquhar and Wing, 2003). Furthermore the trace metal contents of As, Pb and Ni in the "colloform" pyrite resemble the ones measured in ocean-derived Archean sedimentary pyrite (Large et al., 2017).

The siltstone-hosted pyrite show a distinct positive S-isotope signature suggestive of Archean sedimentary sulfides that sourced photochemical-derived reduced sulfur (Farquhar and Wing, 2003). The euhedral shape is likely to be the consequence of a dissolution re-precipitation process in a closed-system as both trace elements and S-isotopes are strongly homogeneous and still typical of sedimentary sulfides.

Ore-related sulfides display a "near-positive" isotopic signature. Such unusual definition has the purpose of highlighting that the $\Delta^{33}S$ signature, although below the 0.15‰, clearly leans to positive side of the $\Delta^{33}S$ axis. Compared with other S-isotope studies on Archean VHMS occurrences, such as the Noranda district (Sharman et al., 2015), the Kidd Creek deposit (Jamieson et al., 2012) or the Teutonic Bore complex (Chen et al., 2015), ore-related sulfides at Nimbus are the ones and only that do not present a mixing relation with sulfur from seawater sulfate. Furthermore, the $\Delta^{33}S$ distribution of the ore-related sulfides, and more directly the positive outliers, is indicative of a contribution, although minor, of sulfur from the intercalated siltstone.

The variable Cd-Hg contents in sphalerite, and in particular the Cd-Hg ratios are suggestive of different fluid compositions among lenses. Such feature may be due to discrete fluid pulses or, in view of the ore distribution in well-defined lenses, to a degree of compartmentalisation of the hydrothermal system.

7 Conclusion

This study reveals a well-defined bimodal fluid evolution of the Nimbus Zn-Ag VHMS deposit. Multiple S-isotope and trace element analyses on "colloform" massive pyrite demonstrate that at first the hydrothermal system formed barren pyritic lenses sourcing the large majority of the sulfur and metals from ocean seawater. The consistent "near-positive" $\Delta^{33}S$ signature from ore-related sulfides indicates that the barren pyrite lenses sealed the hydrothermal system that then evolved sourcing the ore-related sulfur from a deep magmatic source. The positive ore-related $\Delta^{33}S$ outliers suggest only a minor role of sedimentary sulfur in the deposit formation. Finally, trace elements content in sphalerite support a compartmentalised evolution of the system as proposed by Hollis et al. (2017).

Acknowledgements

The authors acknowledge the support of Minerals Research Institute of Western Australia, the Geological Survey of Western Australia, the Australian Research Council through the Centre of Excellence of Core to Crust Fluid Systems and the University of Western Australia through a SIRF scholarship. The authors also acknowledge the facilities, and the scientific and technical assistance of the Australian Microscopy & Microanalysis Research Facility at the Centre for Microscopy, Characterisation & Analysis, the University of Western Australia, a facility funded by the University, State and Commonwealth Governments.

References

Chen M, Campbell IH, Xue Y, et al (2015) Multiple Sulfur Isotope Analyses Support a Magmatic Model for the Volcanogenic Massive Sulfide Deposits of the Teutonic Bore Volcanic Complex, Yilgarn Craton, Western Australia. Economic Geology 110:1411–1423. doi: 10.2113/econgeo.110.6.1411

Duran CJ, Barnes S-J, Corkery JT (2015) Chalcophile and platinum-group element distribution in pyrites from the sulfide-rich pods of the Lac des Iles Pd deposits, Western Ontario, Canada: Implications for post-cumulus re-equilibration of the ore and the use of pyrite compositions in exploration. Journal of Geochemical Exploration 158:223–242. doi: 10.1016/j.gexplo.2015.08.002

Farquhar J, Wing BA (2003) Multiple sulfur isotopes and the evolution of the atmosphere. Earth and Planetary Science Letters 213:1–13. doi: 10.1016/S0012-821X(03)00296-6

Ford A, McCuaig TC (2010) The effect of map scale on geological complexity for computer-aided exploration targeting. Ore Geology Reviews 38:156–167. doi: 10.1016/j.oregeorev.2010.03.008

Hassan LY, Roberts MP (2017) Tellurides associated with volcanogenic massive sulfide (VMS) mineralization at Yuinmery and Austin, Western Australia. Ore Geology Reviews 80:352–362. doi: 10.1016/j.oregeorev.2016.07.005

Hollis SP, Mole DR, Gillespie P, et al (2017) 2.7 Ga plume associated VHMS mineralization in the Eastern Goldfields Superterrane, Yilgarn Craton: Insights from the low temperature and shallow water, Ag-Zn-(Au) Nimbus deposit. Precambrian Research 291:119–142. doi: 10.1016/j.precamres.2017.01.002

Hollis SP, Yeats CJ, Wyche S, et al (2015) A review of volcanic-hosted massive sulfide (VHMS) mineralization in the Archaean Yilgarn Craton, Western Australia: Tectonic, stratigraphic and geochemical associations. Precambrian Research 260:113–135. doi: 10.1016/j.precamres.2014.11.002

Huston DL, Champion DC, Cassidy KF (2014) Tectonic Controls on the Endowment of Neoarchean Cratons in Volcanic-Hosted Massive Sulfide Deposits: Evidence from Lead and Neodymium Isotopes. Economic Geology 109:11–26. doi: 10.2113/econgeo.109.1.11

Jamieson JW, Wing BA, Hannington MD, Farquhar J (2006) Evaluating Isotopic Equilibrium Among Sulfide Mineral Pairs in Archean Ore Deposits: Case Study from the Kidd Creek Vms Deposit, Ontario, Canada. Economic Geology 101:1055–1061. doi: 10.2113/gsecongeo.101.5.1055

Johnston DT (2011) Multiple sulfur isotopes and the evolution of Earth's surface sulfur cycle. Earth-Science Reviews 106:161–183. doi: 10.1016/j.earscirev.2011.02.003

LaFlamme C, Martin L, Jeon H, et al (2016) In situ multiple sulfur isotope analysis by SIMS of pyrite, chalcopyrite, pyrrhotite, and pentlandite to refine magmatic ore genetic models. Chemical Geology 444:1–15. doi: 10.1016/j.chemgeo.2016.09.032

Large RR, Mukherjee I, Gregory DD, et al (2017) Ocean and Atmosphere Geochemical Proxies Derived from Trace Elements in Marine Pyrite: Implications for Ore Genesis in Sedimentary Basins. Economic Geology 112:423–450. doi: 10.2113/econgeo.112.2.423

Mole DR, Fiorentini ML, Cassidy KF, et al (2013) Crustal evolution, intra-cratonic architecture and the metallogeny of an Archaean craton. Geological Society, London, Special Publications

393:SP393.8. doi: 10.1144/SP393.8
Sharman ER, Taylor BE, Minarik WG, et al (2015) Sulfur isotope and trace element data from ore sulfides in the Noranda district (Abitibi, Canada): implications for volcanogenic massive sulfide deposit genesis. Miner Deposita 50:591–606. doi: 10.1007/s00126-014-0559-7